2016

Development of a compact vertical-cavity surface-emitting laser end-pumped actively Q-switched laser for laser-induced breakdown spectroscopy

Shuo Li
University of Pittsburgh

L. Liu
University of Nebraska-Lincoln, lliu1@unl.edu

Rongzhang Chen
University of Pittsburgh

Bryan Nelsen
University of Pittsburgh

Xi Huang
University of Nebraska-Lincoln

See next page for additional authors

Authors
Shuo Li, L. Liu, Rongzhang Chen, Bryan Nelsen, Xi Huang, Yongfeng Lu, and Kevin Chen

REVIEW OF SCIENTIFIC INSTRUMENTS **87**, 033114 (2016)

Development of a compact vertical-cavity surface-emitting laser end-pumped actively Q-switched laser for laser-induced breakdown spectroscopy

Shuo Li,[1] Lei Liu,[2] Rongzhang Chen,[1] Bryan Nelsen,[1] Xi Huang,[2] Yongfeng Lu,[2] and Kevin Chen[1,a)]

[1]*Department of Electrical and Computer Engineering, University of Pittsburgh, Pittsburgh, Pennsylvania 15260, USA*

[2]*Department of Electrical and Computer Engineering, University of Nebraska-Lincoln, Lincoln, Nebraska 68588, USA*

(Received 6 January 2016; accepted 13 March 2016; published online 30 March 2016)

This paper reports the development of a compact and portable actively Q-switched Nd:YAG laser and its applications in laser-induced breakdown spectroscopy (LIBS). The laser was end-pumped by a vertical-cavity surface-emitting laser (VCSEL). The cavity lases at a wavelength of 1064 nm and produced pulses of 16 ns with a maximum pulse energy of 12.9 mJ. The laser exhibits a reliable performance in terms of pulse-to-pulse stability and timing jitter. The LIBS experiments were carried out using this laser on NIST standard alloy samples. Shot-to-shot LIBS signal stability, crater profile, time evolution of emission spectra, plasma electron density and temperature, and limits of detection were studied and reported in this paper. The test results demonstrate that the VCSEL-pumped solid-state laser is an effective and compact laser tool for laser remote sensing applications. © *2016 AIP Publishing LLC.* [http://dx.doi.org/10.1063/1.4944856]

I. INTRODUCTION

Laser-induced breakdown spectroscopy (LIBS) is a powerful diagnostic technique for the determination of elemental compositions of specimens in gaseous, liquid, and solid phases.[1,2] As a real-time and convenient analytical tool, LIBS has been widely used in laboratories. Research and development efforts invested in the last two decades have yielded a number of enhanced LIBS techniques with excellent sensitivity and accuracy.[3–6] As the performance of LIBS evolves in laboratories, there is increasing focus on the development of portable LIBS instruments for use in the field as stand-off sensing tools for harsh or dangerous environments.[7–9] This has been hindered by the lack of compact, high efficiency, and highly reliable lasers that can produce plasmas with sufficient optical emission.

Over the last decade, a number of miniaturized solid-state lasers have been demonstrated to deliver sufficient laser pulse energy with necessary peak intensity to perform LIBS analysis.[10] Most of these laser systems are Q-switched solid-state lasers. Besides the laser performance itself, dimension, weight, and efficiency are the key requirements for portable laser applications. Despite advances in these compact laser sources, some compromises have to be made. For example, microchip lasers usually have low pulse energies and work in the passively Q-switch mode, making them inappropriate to perform time-resolved measurements due to their poor jittering.[11] In order to achieve a breakdown threshold using microchip lasers, tight focusing is essential, which drastically reduce the stand-off distance.[10] Compact flash lamp pumped lasers, on the other hand, have high pulse energies and can be synchronized with spectrometers to perform time-resolved measurements. However, pumping with a spectrally wide flash lamp is not as efficient because most of the pumping energy is turned into heat instead of pumping the gain medium. A more energy-efficient pumping scheme is the diode laser pumping enabled by high-power edge-emitting diode laser stacks and vertical-cavity surface-emitting lasers (VCSELs).

Both side and end pumping schemes have been used to achieve lasing using diode pump lasers. However, the end pumping scheme has been widely used for compact solid-state lasers for its high energy absorption efficiency. The pumping light profile can be adjusted to coincide with the cavity resonator mode to yield good laser beam quality. In the past, the end-pumping scheme for compact solid-state lasers for LIBS applications was achieved using a stack of edge-emitting laser diodes.

Recently, a new class of high-power VCSEL devices have been developed as laser pump sources. Comparing with the edge-emitting laser stacks, VCSELs have high efficiency (>40%).[12] The narrow linewidth of VCSEL (1 nm, full width at half-maximum (FWHM)) enables strong and resonate absorption of Nd: YAG crystal.[13] These two factors guarantee a high overall battery efficiency of the lasers. The cooling schemes for VCSEL chips are straightforward. This ensures a far smaller overall packaging size than those of edge-emitting laser stacks, making them suitable as a pump source for compact lasers. VCSELs have a uniform output profile, which enable good laser beam profile. This is crucial for LIBS applications. Because of these advantages, the VCSEL laser chips have become popular pumping sources for compact solid-state laser developments and applications such as mid-IR conversion[14] and laser spark plugs.[15]

[a)]Author to whom correspondence should be addressed. Electronic mail: pec9@pitt.edu

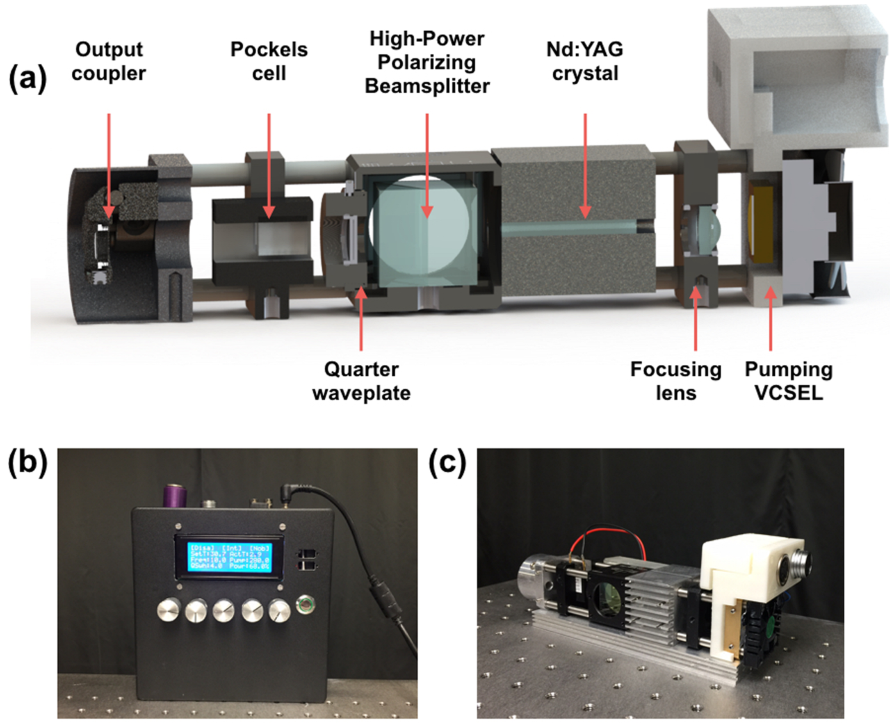

FIG. 1. Laser schematic and photos. (a) Schematic of the laser cavity design, (b) photo of the laser controller, and (c) photo of the laser body.

In this paper, we describe the development of a compact actively Q-switched Nd:YAG laser end-pumped by a high-power VCSEL chip. The performance of this compact laser and its LIBS applications was studied. To our best knowledge, this is the first time that such a laser is utilized in LIBS applications. The laser operated at the wavelength of 1064 nm with a maximum pulse energy of 12.9 mJ. The repetition rate can be varied from 1 to 200 Hz. The laser performance was first studied, including output power, pulse width, timing jitter, pulse stability, and Q-switch delay. Then the laser was used to perform several LIBS experiments in order to compare our results with a number of previous studies which utilized other laser sources. Crater profiles, time evolution of emission spectra, plasma electron density and temperature, and limits of detection (LODs) were studied as quantitative analyses of several NIST Standard Reference Materials (SRM) alloy samples.

II. LASER DESIGN

The laser cavity design is shown in Fig. 1(a). The laser crystal is end pumped by a VCSEL array,[16] which has an output wavelength of 806.9 nm and a maximum output power of 800 W. The VCSEL operates in a quasi-cw mode with a maximum pulse duration of 300 μs. A single lens with a 10 mm focal length was used to couple the pumping light into a laser rod through one end of the rod. This end also acts as one reflector of the laser cavity. The Nd:YAG rod has an anti-reflection coating for the pumping wavelength of 806.9 nm and a high-reflection coating for the lasing wavelength of 1064 nm on the end facing the VCSEL. On the other end of the rod, there is an anti-reflection coating for the lasing wavelength. A high-power polarizing beam splitter, a quarter-wave plate, and a Pockels cell work together as an active Q-switch. An output coupler with a transmission of 50% acts as the other end of the laser cavity. The length of this cavity is about 14 cm. All opto-mechanic components of the lasers were housed in a 30 mm cage.

The laser controller is shown in Fig. 1(b). The electronic and timing control system of the laser was centered around a low-power Atmega328 microcontroller with a 16 MHz clock speed. To operate this actively Q-switched laser, Transistor–transistor logic (TTL) pulses provided by the microcontroller were used to control the triggering of the VCSEL and the Pockels cell. The microcontroller at this clock speed is adequate to synchronize multiple lasers and spectrometers with sufficient timing accuracy to perform time-resolved or

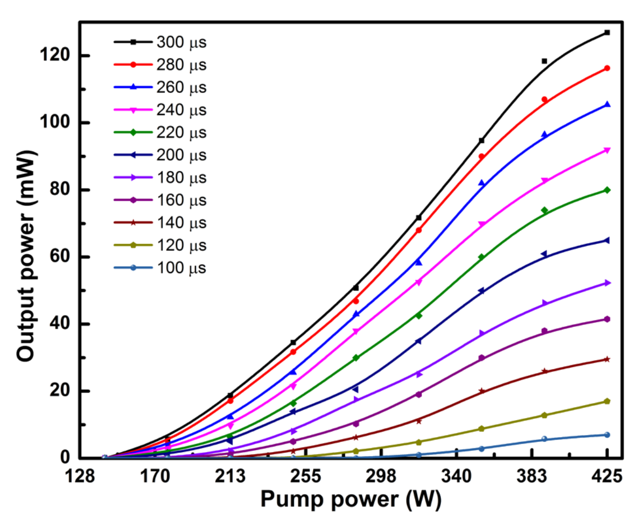

FIG. 2. Output power vs. pump power at various pump durations. The laser was running at 10 Hz.

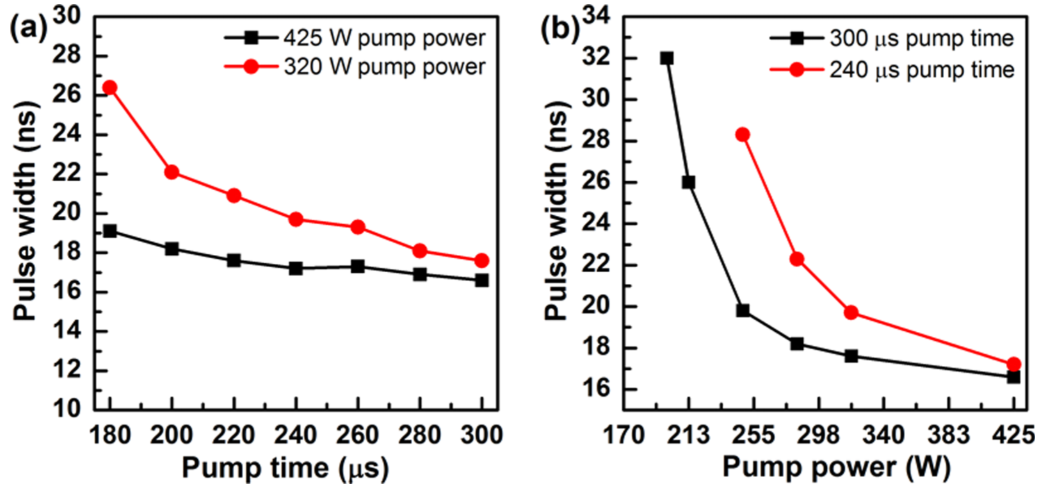

FIG. 3. Laser pulse width measurement. (a) Pulse width as a function of pump time at two different pump powers, and (b) pulse width as a function of pump power at two different pump times.

dual-pulse LIBS for high sensitivity measurements of ionic (<1 μs) and atomic (<20 μs) optical emissions. Because of VCSEL's high pumping efficiency, the laser crystal can be air cooled to avoid water cooling. The power supply in this laser control system was able to produce a 425 W peak output power of the VCSEL. The temperature of the VCSEL itself is controlled by a Peltier cell and a fan, which enables the laser to work at a maximum 200 Hz repetition rate. This is a significant improvement from the flash lamp based solid-state lasers for the LIBS applications, which only allow 2 Hz repetition rate.[17] The wall-plug power efficiency of the pumping VCSEL is 34%. The VCSEL input to laser output efficiency is about 10%. This gives a 3.4% of total electrical-to-optical efficiency.

The laser head shown in Fig. 1(c) has a dimension of 60 $\times$ 60 $\times$ 170 mm^3 and weighs about 0.7 kg. The laser controller as shown in Fig. 1(b) has a compact size of 200 $\times$ 200 $\times$ 60 mm^3 and weighs about 1.7 kg. Since the whole laser system is air cooled, no water chiller is needed. The system runs at 24 V DC.

III. LASER CHARACTERISTICS

A. Output power

The laser output power was first studied at various pump conditions with the laser running at 10 Hz. The output power was measured using a thermal power meter (Thorlabs, S302C). As is shown in Fig. 2, the laser output power was characterized at different pump powers and durations. The pump threshold was measured at 130 W. After reaching the pump threshold, the laser output power increases with the pump power and the slope also increases with the pump duration. The maximum output power of the laser is limited by the electronics used to power the pump VCSEL, which was capped at 425 W or 53% of the maximum output power of the VCSEL. This yields a maximum output pulse energy of 12.9 mJ/pulse.

B. Pulse width

Laser pulse width (FWHM) was also studied under various pump conditions. The laser pulse was attenuated using

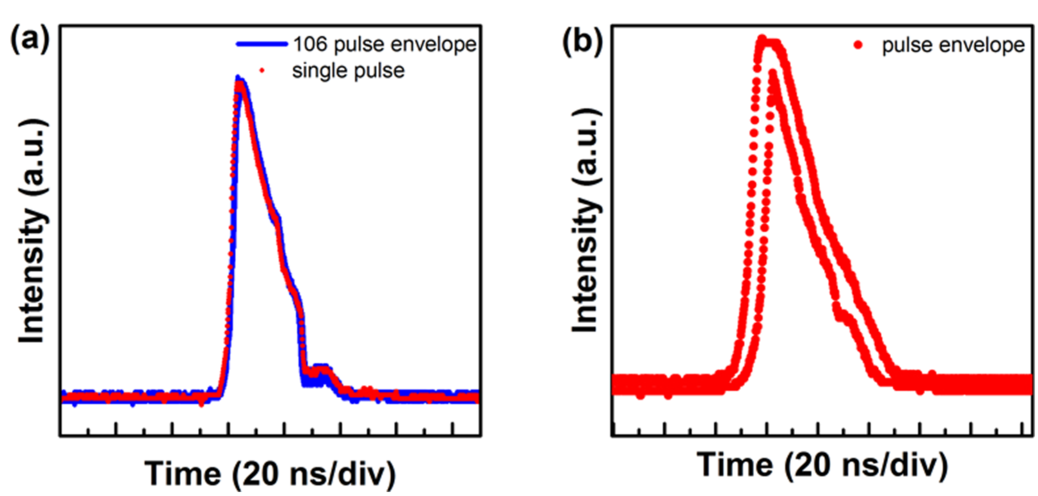

FIG. 4. Laser shot-to-shot pulse stability and timing jitter. (a) Stability measurements of laser pulse by comparing the envelope formed by 106 pulses and a single pulse. (b) Laser timing jitter measurements by analyzing the pulse envelope formed by 106 pulses. The pulse energy is 12.9 m/pulse and the repetition rate is 10 Hz.

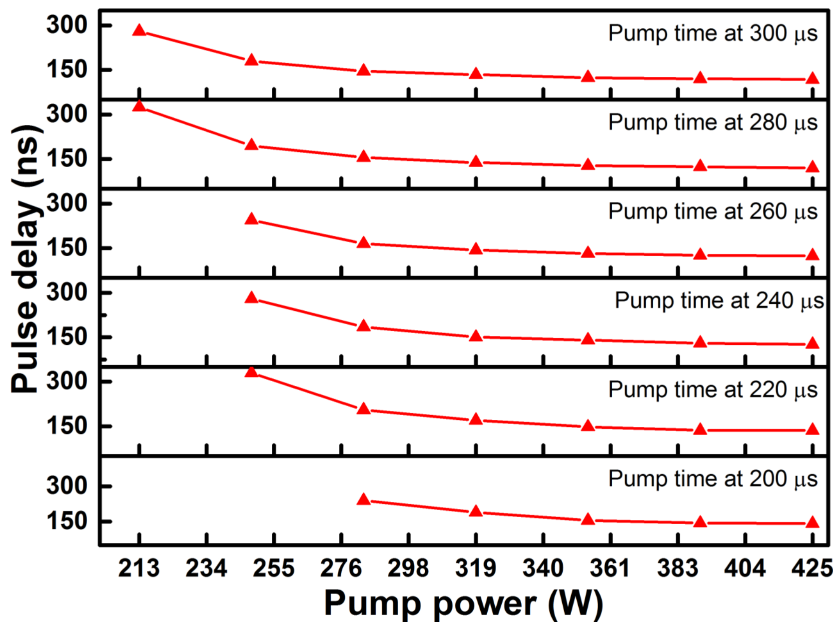

FIG. 5. Pulse delays as functions of the pump power at various pump times.

a high power polarizer, a half wave plate, and a neutral density filter to avoid damaging photodiode. The attenuated pulse was then measured by a high speed InGaP photodiode (New Focus 1544-B) connected to a digital oscilloscope with a bandwidth of 2.5 GHz (DPO7254, Tektronix). Pulse width as functions of pump durations at two different VCSEL pump power of 425 and 320 W is presented in Fig. 3(a). Output laser pulse width decreases when the pumping duration increases from 180 to 300 μs. The pulse width was reduced to 16.6 and 17.6 ns, respectively. The output pulse width can be further reduced when the pump duration was increased. Fig. 3(b) shows the relationship between the pulse width and the VCSEL pump power when the pump duration was set at 240 and 300 μs, respectively. For a fixed pump time, the pulse width decreases with increased pump power. Characteristics presented in Fig. 3 are consistent with a previous report.[17]

C. Laser stability and timing jitter

Laser shot-to-shot pulse stability and timing jitter are very important parameters to ensure reliable LIBS measurements. Pulse stability was studied by recording continuous pulse shape as an envelope using the oscilloscope. A pulse envelope formed by 106 pulses was plotted in Fig. 4(a) (blue traces). It is compared with a pulse shape of a single laser shot (red dot). Result presented in Fig. 4(a) shows that the peak intensity variation of 106 pulses is less than 1%, demonstrating the high stability of the laser pulses.

The timing jitter measurement was shown in Fig. 4(b), where a 10 Hz signal from the microcontroller was sent to the oscilloscope channel 1 as trigger, while the pulse signal measured by the photodiode was fed to the oscilloscope channel 2. 106 continuous pulses were recorded to form a pulse envelope with the outline shown in red dot. By studying the pulse envelope width, timing jitter was estimated to be ±2 ns, comparable to most actively Q-switched lasers.

D. Q-switch delay

An important parameter of actively Q-switched lasers for time-resolved LIBS measurements is the Q-switch delay. At the end of VCSEL pumping pulse, a trigger signal is sent to Pockels cell. The laser pulse will not emit until after a time delay, during which time the pulse builds up exponentially from noise. This delay is referred as the Q-switch delay. This is presented in Fig. 5, where the Q-switch delays were measured for the VCSEL pump durations from 200 to 300 μs with pump powers ranging from 213 to 425 W. The Q-switch delay times were found to be between 120 and 325 ns. At the peak pump power of 425 W, the Q-switch delay time reduced to the minimal of 120 ns at the pump duration of 300 μs. When the pump duration decreased to 200 μs,

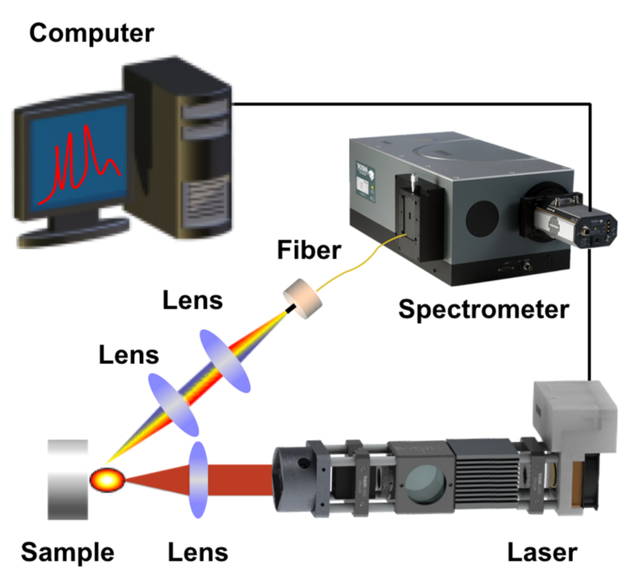

FIG. 6. Schematic of LIBS setup.

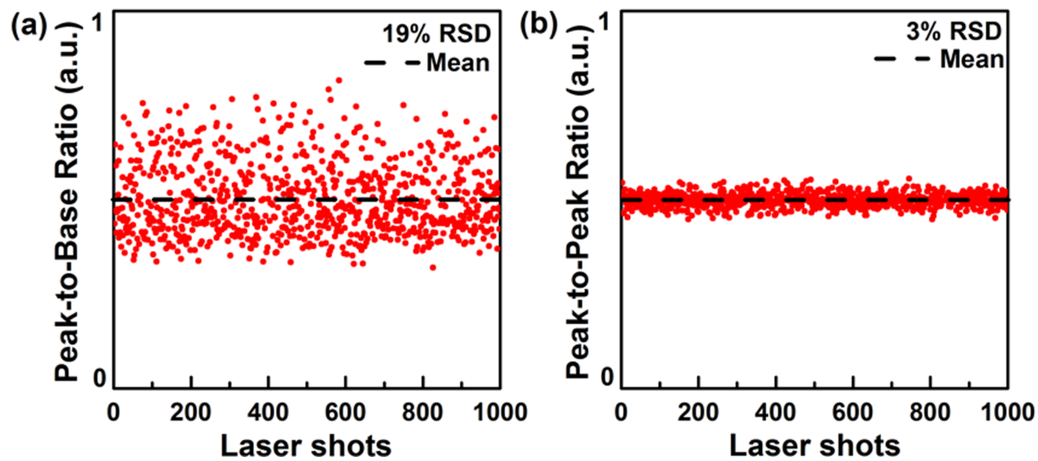

FIG. 7. Shot-to-shot emission peak analysis. (a) Al 396.2 peak-to-base atomic emission ratios for a 1000-shot sequence. (b) Al394.5/Al396.2 peak-to-peak atomic emission ratios for a 1000-shot sequence. Each data point is represented by a red dot. The black dashed line shows the average value. The gate width was set at 50 ns and the gate delay was set at 500 ns.

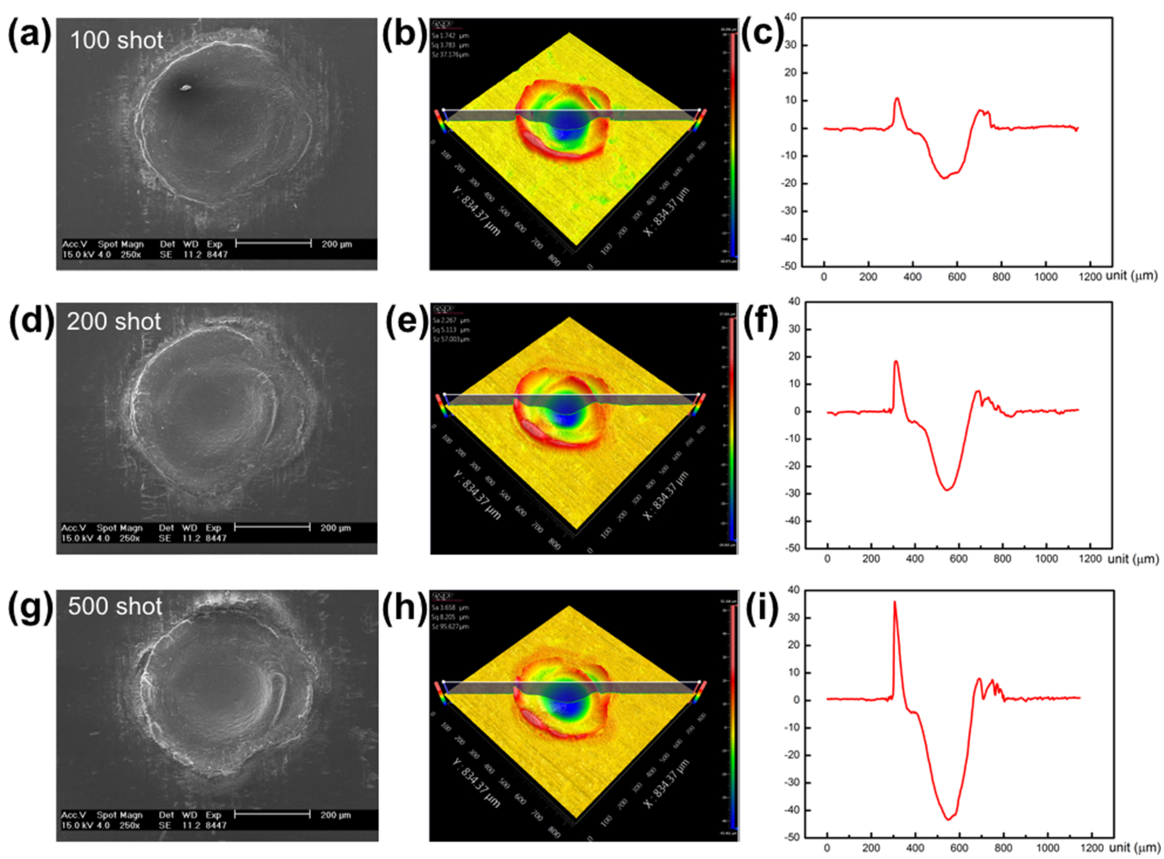

FIG. 8. Crater created by different numbers of focused laser pulses. (a), (d), and (g) SEM image of craters created by 100, 200, and 500 laser pulses. (b), (e), and (h) 3D images of craters. (c), (f), and (i) Crater cross sections obtained from 3D images.

TABLE I. Ablation efficiency at different numbers of pulses.

Number of pulses	10	50	100	200	500
Ablation efficiency (μm^3/mJ)	1.76	0.52	0.42	0.20	0.20

the minimal Q-switch delay was measured as 136 ns. The result obtained here was used to calibrate synchronization between the laser and the spectrometer when performing LIBS experiments.

IV. LIBS EXPERIMENT

A. LIBS experiment setup

The schematic of LIBS setup is shown in Fig. 6. The compact laser operated at its fundamental wavelength (1064 nm) with a pulse repetition rate of 10 Hz. The output pulse had a pulse energy of 12.9 mJ and a pulse width of 16.6 ns. The Pockels cell's triggering signal was also used to synchronize with the spectrometer (Andor Tech., Shamrock 505i), which was equipped with an intensified charge coupled

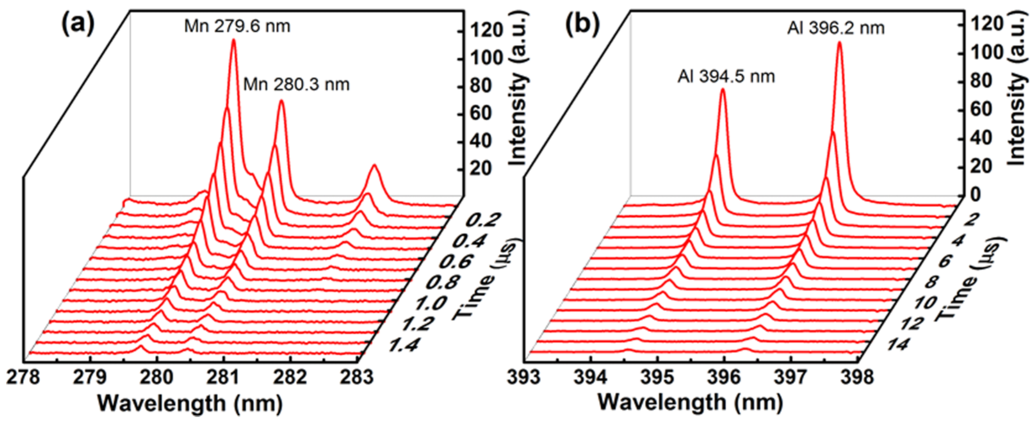

FIG. 9. Time-resolved emission spectra of an Al alloy sample. (a) Mg ionic line with gate width set at 100 ns. (b) Al atomic line with gate width set at 1000 ns. Each spectrum was averaged over 30 pulses.

device (ICCD) detector (Andor Tech., iStar, DT-334T). The 120 ns Q-switch delay was taken into account for the synchronization. The optical emissions from the plasmas were coupled into a fiber bundle which is connected to the spectrometer by two lenses (6 and 10 cm focal lengths). The laser beam was focused onto the sample surface by a single lens (20 cm focal length). The focused spot size is around 0.3 mm. The sample itself was mounted on a computer-controlled motorized stage that moved the sample during the measurement to avoid over ablation.

B. LIBS shot-to-shot signal stability

Shot-to-shot stability of LIBS signals is an indirect reflection of variations in laser performance such as pulse energy stability and timing jitter. The laser pulse was focused on an aluminum alloy sample (NIST SRM 1259) to generate plasmas. The strong Al 394.4 nm and Al 396.2 nm atomic emission lines were chosen to minimize the effect of inhomogeneity on precision. A series of 1000 sequential LIBS spectra were recorded to study the peak-to-base and peak-to-peak ratios. As can be seen in Fig. 7(a), the Al 396.2 nm peak-to-base ratios had a relative standard deviation (RSD) of 19%, which was comparable to the previous study[18] but obtained with only 10% of its pulse energy. This RSD was mainly determined by the target surface quality at the point of analysis. The peak-to-peak (Al 394.4/Al 396.2) atomic line emission ratios, as shown in Fig. 7(b), had a RSD of 3%. Both of the shot-to-shot signal stability tests above have demonstrated that our laser has excellent performance in terms of LIBS measurement repeatability.

C. Crater profiles and ablation efficiency

The experiments were performed without using any spatial filter to optimize the beam profile. The laser pulse was directly focused onto the sample surface by a single lens (20 cm focal length). Craters formed by 10, 50, 100, 200, and 500 laser pulses on a stainless steel sample (NIST 304) were studied using a scanning electron microscope (SEM) and a white light interferometric microscope (Zygo). SEM images of three craters formed by 100, 200, and 500 pulses are shown in Figs. 8(a), 8(d), and 8(g), respectively, and the corresponding 3D images generated from the interferometric scope are shown

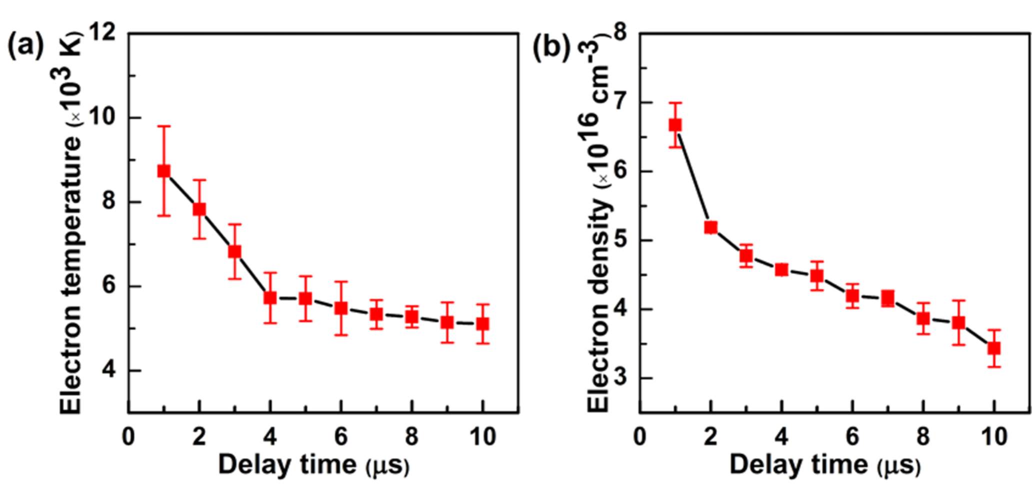

FIG. 10. Time evolution of electron temperature (a) and electron density (b) in laser induced plasma. The gate width was set at 1 μs. Each spectrum was averaged over 30 pulses.

TABLE II. Elemental concentrations (wt. %) of Mn and Cr in Al alloy sample.

	Standard reference materials (wt. %)				
Elements	1255b	1256b	1240C	1258I	No.1259
Mn	0.0527	0.3857	1.2680	0.4810	0.0790
Cr	0.0150	0.0572	0.000 54	0.0011	0.1730

in Figs. 8(b), 8(e), and 8(h). The crater profiles obtained here were prominently cone-like because of the almost perfect Gaussian laser beam profiles.[19] The spike structures around the edge of the craters were formed by the recondensation of the plasmas. Figs. 8(c), 8(f), and 8(i)) show the cross sections of these craters, which were then used to estimate the crater volumes. The ablation efficiency is defined as the ratio of the crater volume to the laser pulse energy. The ablation efficiency of different numbers of pulses is shown in Table I. As the number of pulses increased, the ablation efficiency decreased. The ablation efficiency from the first 10 pulses was about 1.76 μm^3/mJ, which reduced to 0.2 μm^3/mJ for 500 pulses.

D. Time-resolved emission spectra

Time-resolved measurements can provide a detailed diagnostic of the transient plasmas. Time-resolved emission spectra for an aluminum alloy sample (NIST 1259) are shown in Fig. 9, where Fig. 9(a) shows Mg ionic emission lines (279.6 and 280.3 nm) and Fig. 9(b) shows Al atomic emission lines (394.5 and 396.2 nm). A monoexponential temporal behavior was observed for the emission peak intensity. An exponential curve fitting algorithm was used to calculate the lifetime of each peak. The lifetimes of 279.6, 280.3, 394.5, and 396.2 lines were calculated to be 0.66 ± 0.048, 0.62 ± 0.023, 1.67 ± 0.11, and 1.62 ± 0.11 μs, respectively. The plasma lifetimes obtained here were at least a thousand times longer than those obtained by a microchip laser.[11]

E. Electron temperature and density

The plasma temperature and electron density can be obtained through time-resolved emission spectra. Atomic lines of Al I 309.28 nm and Al I 396.15 nm were chosen to evaluate the electron temperature based on the assumption of local thermodynamic equilibrium.[20] As shown in Fig. 10(a), the plasma temperatures were estimated to be 5000 K–8000 K from 2 to 10 μs. Electron density, on the other hand, was evaluated from the Stark broadening.[20] The Al I 396.2 nm atomic line was chosen to measure the FWHM line width for evaluating the electron densities. As shown in Fig. 10(b), the electron densities were on the order of 10^{16} cm^{-3} from 1 to 10 μs. Since the property of the laser-induced plasmas depends on several factors such as laser wavelength, laser energy, pulse duration, and the sample, it is very difficult to compare the results obtained here with other results. But the results generally appear similar to our previous studies.[5,21]

F. LOD measurements

Five Aluminum standard reference materials from NIST were used as targets in this study. The concentration details are listed in Table II. LODs were calculated according to International Union of Pure and Applied Chemistry (IUPAC) criterion: LOD = 3 σ/s, where σ is the standard deviation of the background and s is the slope of the calibration curve. The emission lines chosen to construct the calibration curves here are Cr I 367.87 nm, Mn I 403.07, and Al I 309.28 nm. Fifteen measurements were performed to produce the calibration curves. As shown in Fig. 11, the obtained calibration curves have good linear fitting (R > 98%) within the experimental uncertainty. The estimated LODs for trace elements of Cr and Mn were 101 and 192 ppm, respectively. The LODs obtained here were comparable to those reported in previous researches using a commercial actively Q-switched Nd:YAG laser.[22] It should be pointed out that the results obtained here are specific to the experimental setup. The main objective here is not to improve LODs but to evaluate the laser performance in LIBS.

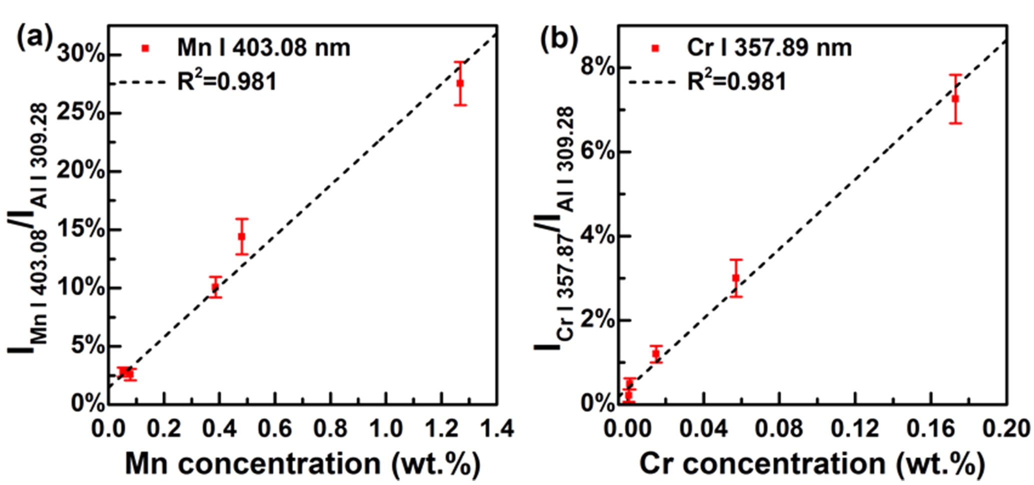

FIG. 11. Calibration curves for (a) Mn (403.08 nm) and (b) Cr (357.89 nm) in aluminum samples. A gate delay of 1 μs and gate width of 10 μs were used for acquisition. Total number of 30 pulses were accumulated during each measurement.

V. CONCLUSION

The new laser source developed in this study not only exhibits high laser performance but also meets the dimension, weight, and efficiency requirements of a field portable laser source for LIBS applications. Time-resolved LIBS measurements were successfully performed using this laser combined with an ICCD detector. Reliable LIBS results were obtained from such experiments.

Although similar laser design has been demonstrated before, the work undertaken for this study has resulted in a truly compact, lightweight, and high performance laser. Furthermore, the laser runs at 24 V DC, making it possible to be powered by a battery. Most of the laser body is built from commercially available parts. Its weight and dimensions can be further reduced by using 3D-printing technology, making it more attractive for LIBS applications.

ACKNOWLEDGMENTS

This research work was financially supported by Defense Threat Reduction Agency (through No. HDTRA1-12-1-0019). We would like to thank Tong Chen for his support in the laser design. We would also like to thank Thorin Tobiassen for his help in laser part development.

[1]D. A. Rusak, B. C. Castle, B. W. Smith, and J. D. Winefordner, Crit. Rev. Anal. Chem. **27**, 257 (1997).
[2]E. Tognoni, V. Palleschi, M. Corsi, and G. Cristoforetti, Spectrochim. Acta, Part B **57**, 1115 (2002).
[3]C. Gautier, P. Fichet, D. Menut, and J. Dubessy, Spectrochim. Acta, Part B **61**, 210 (2006).
[4]H. H. Telle, D. C. S. Beddows, G. W. Morris, and O. Samek, Spectrochim. Acta, Part B **56**, 947 (2001).
[5]L. Liu, S. Li, X. N. He, X. Huang, C. F. Zhang, L. S. Fan, M. X. Wang, Y. S. Zhou, K. Chen, L. Jiang, J. F. Silvain, and Y. F. Lu, Opt. Express **22**, 7686 (2014).
[6]Y. Ikeda, A. Moon, and M. Kaneko, Appl. Opt. **49**, C95 (2010).
[7]V. Lazic, A. Palucci, S. Jovicevic, and M. Carpanese, Spectrochim. Acta, Part B **66**, 644 (2011).
[8]M. Civis, S. Civis, K. Sovova, K. Dryahina, P. Spanel, and M. Kyncl, Anal. Chem. **83**, 1069 (2011).
[9]A. Sarkar, D. Alamelu, and S. K. Aggarwal, Appl. Opt. **47**, G58 (2008).
[10]J. Rakovsky, P. Cermak, O. Musset, and P. Veis, Spectrochim. Acta, Part B **101**, 289 (2014).
[11]I. B. Gornushkin, K. Amponsah-Manager, B. W. Smith, N. Omenetto, and J. D. Winefordner, Appl. Spectrosc. **58**, 762 (2004).
[12]R. Van Leeuwen, Y. Xiong, J.-F. Seurin, G. Xu, A. Miglo, Q. Wang, B. Xu, W.-X. Zou, D. Li, J. D. Wynn, V. Khalfin, and C. L. Ghosh, Proc. SPIE **8381**, 83810I (2012).
[13]R. V. Leeuwen, Y. Xiong, L. S. Watkins, J.-F. Seurin, and G. Xu, Proc. SPIE **7912**, 79120Z (2011).
[14]I. Vurgaftman, J. R. Meyer, and L. R. Ram-Mohan, IEEE J. Quantum Electron. **34**, 147 (1998).
[15]E. Wintner, H. Kofler, D. K. Srivastava, and A. K. Agarwal, Proc. SPIE **9065**, 90650B (2013).
[16]L. Goldberg, C. McIntosh, and B. Cole, Opt. Express **19**, 4261 (2011).
[17]J. Goujon, A. Giakoumaki, V. Pinon, O. Musset, D. Anglos, E. Georgiou, and J. P. Boquillon, Spectrochim. Acta, Part B **63**, 1091 (2008).
[18]B. C. Castle, K. Talabardon, B. W. Smith, and J. D. Winefordner, Appl. Spectrosc. **52**, 649 (1998).
[19]O. V. Borisov, X. L. Mao, and R. E. Russo, Spectrochim. Acta, Part B **55**, 1693 (2000).
[20]S. N. T. Jagdish and P. Singh, *Laser-Induced Breakdown Spectroscopy* (Elsevier, 2007).
[21]L. B. Guo, C. M. Li, W. Hu, Y. S. Zhou, B. Y. Zhang, Z. X. Cai, X. Y. Zeng, and Y. F. Lu, Appl. Phys. Lett. **98**, 131501 (2011).
[22]M. A. Ismail, G. Cristoforetti, S. Legnaioli, L. Pardini, V. Palleschi, A. Salvetti, E. Tognoni, and M. A. Harith, Anal. Bioanal. Chem. **385**, 316 (2006).